Supplemental Information to

Designing Molecular Structure to Achieve Ductile Fracture Behavior in a Stiff and Strong 2D Polymer, "Graphylene"

Emil Sandoz-Rosado, Todd D. Beaudet, Rad Balu, Eric D. Wetzel*

U.S. Army Research Laboratory, Materials and Manufacturing Sciences Division

Aberdeen Proving Ground, MD 21005

*eric.d.wetzel2.civ@mail.mil, 410-306-0851

Density Functional Theory Method Details

The density functional theory (DFT) **[SR1-2]** calculations were completed using the CP2K computer code **[SR3]**. This code employs the Quick-Step method outlined by VendeVondele *et al*. **[SR4]** which uses a Gaussian basis for the single-body functions (i.e. molecular orbitals) and a plane-wave multi-grid basis for the electron density. Within this framework we use the generalized gradient approximation exchange-correlation functional BLYP due to Becke **[SR5]** and Lee, Yang, Parr **[SR6]**. Pseudopotentials developed by Goedecker, Teter, and Hutter (GTH) **[SR7-8]** and optimized for BLYP by Krack **[SR9]** are used for both carbon and hydrogen. The Gaussian basis fit for BLYP/GTH uses double-zeta and valence polarization functions while the plane-wave basis uses a 350 Ry cutoff. In all calculations the Gamma point of the Brillioin zone is treated using a 96 atom super cell. Periodic boundary conditions are used in all three dimensions such that the membrane sheets are spaced by 15 Å. Dispersion interactions are accounted for using the DFT-D method with D3 parameterization as implemented in CP2K **[SR10-11]**. Total energies, energy gradients and stress tensor elements were converged to less than 1.0×10^{-6} Hartree, 4.5×10^{-4} Hartree/bohr, and 100 bar respectively throughout.

Molecular Dynamics Method Details

Molecular dynamics simulations were executed using the LAMMPS software package **[SR 12]**. Graphene and graphylene unit cells were obtained from DFT calculations and then propagated into larger domains for MD simulation. The REBO potential was used **[SR 13]** with a time step of 1fs and a potential cutoff of 0.197nm for accurate carbon-carbon bond scissioning **[SR14-16]** for all scenarios. Uniaxial tension tests were performed by time integrating under constant energy with an initial temperature condition of 0K and displacing the edges of the domain at a constant strain rate. Quasi-static fracture toughness tests were later performed by initializing the domain at either 0K or 300K using a Berendsen thermostat, then releasing the thermostat and time integrating with a constant energy for the domain. Once the domains for the fracture toughness simulations were thermalized, a crack was induced by deleting atoms in the center of the domain and the edges of the domain were displaced at constant strain rates of $0.167ns^{-1}$ and $2.0ns^{-1}$. Dynamic crack propagation tests were performed by imposing a 0K and 5% strain initial condition along the direction of stretching. The 5% strain at the edge of the domain was held constant and the domain was then time integrated under constant energy. Energy release rate was determined by measuring the system potential energy and crack length at various integration times. Crack length

was determined by finding the two points of concentration of stress parallel to the direction of stretching.

Prioritization of GrE-2 Graphylene Relative to Other GrE-*n* Graphylenes

We define graphylene-n (GrE-n) as a graphene-polyethylene hybrid 2D polymer, where *n* indicates the characteristic length of the polyethylene (PE) chains in terms of the number of methylene bridge units (-CH_2-) between each nearest neighbor C_6 ring. Stoichiometrically, GrE-*n* has a C:H ratio of 2+*n*:2*n* so that a higher *n* has a lower fraction carbon content approaching that of PE. Also, the smallest possible GrE-*n* primitive cell has 6+9*n* atoms.

We considered GrE structures with both odd and even *n*. However, the hexagonal symmetry of graphylene can accommodate the methylene bond angles more deterministically for even *n*. Consider that each sp^3 bond pair surrounding a single methylene C atom wishes to form an angle, so the bond will have either a R-handed or L-handed chiral character for GrE structures with largely in-plane C atoms ("R" and "L" refer to "right" and "left"). Alternatively, for GrE structures with C atoms located out-of-plane, these bonds could be U-oriented or D-oriented ("U" and "D" refer to "up" and "down"). We consider the latter case in detail although similar arguments can be made for the former case.

Figure S1 compares symmetric arrangements of U and D bonds for representative GrE-1 and GrE-2 systems. Subfigure S1a shows an oblique GrE-1 with UUDDUD methylene orientations cycling the C_6 rings; subfigure S1b alternatively shows a rectangular GrE-1 where each C_6 is cycled by either UUUDUD or DDDUDU. It is immediately noticed that one cannot use the minimal 15 atom primitive, otherwise the membrane will have more hydrogen on one side than the other. Thus, such GrE-1 constructions need at least 30 atoms which is more than the 24 atom primitive of GrE-2. Similar arguments require such GrE-3 primitive constructions to have at least 66 atoms. On the other hand, Fig. S1c shows a minimal GrE-2 primitive can allow construction of hexagonal symmetry using UDUDUD orientations; and Fig. S1d shows rectangular symmetry using UUUDDD orientations. In this way odd GrE-*n* is somewhat frustrated, requiring larger simulation cells and more extensive conformal searches while still not accessing higher symmetries readily available in the GrE-2 class of membranes. Thus we favor GrE-2 as a first step in characterizing GrE physics, and will present odd GrE-*n* systems in a future study.

Within the even *n* graphylene family, GrE-2 is prioritized for study as the structure most similar to graphene.

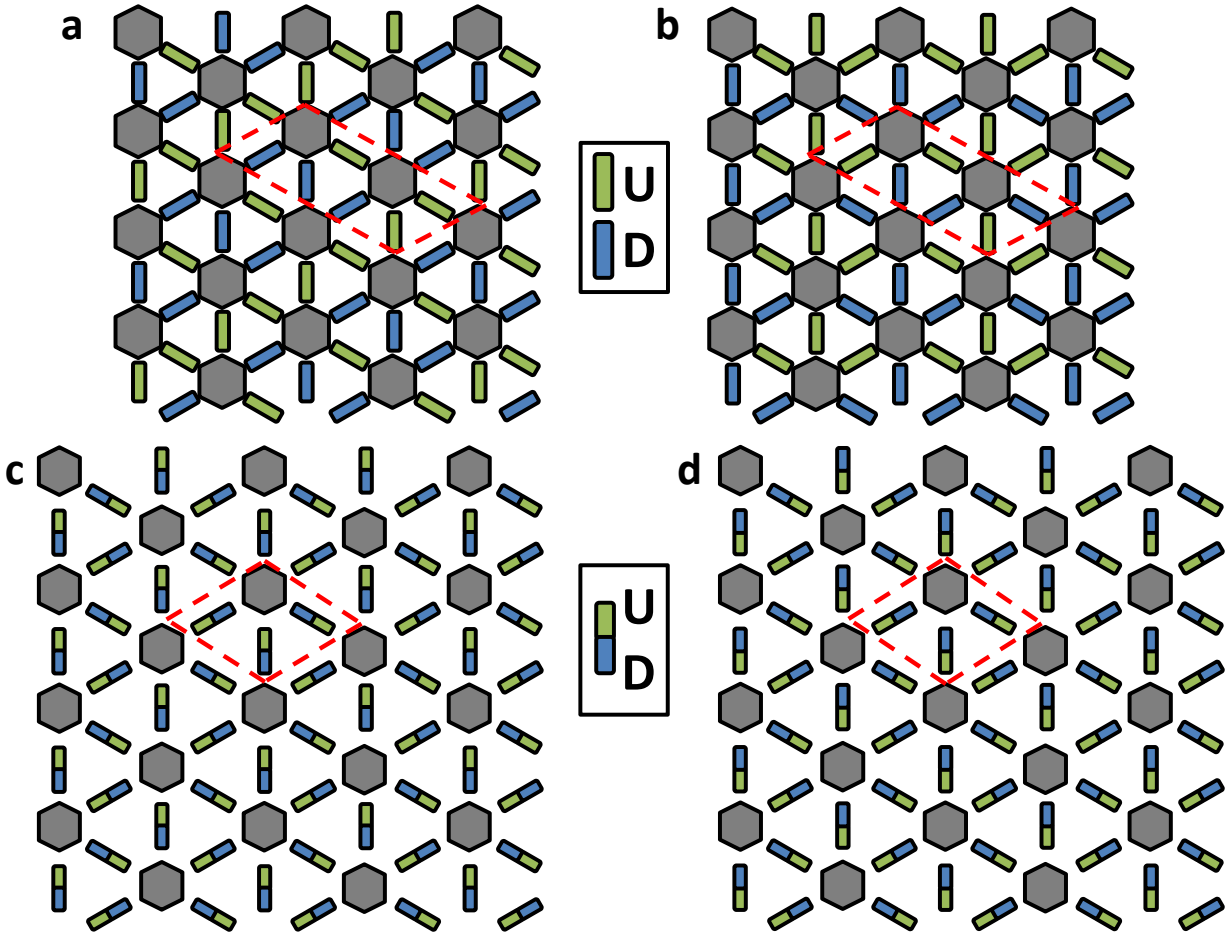

Figure S1. Comparison of simplest unit cells for GrE-1 and GrE-2 structures, for out-of-plane configurations with C atoms in the PE chains permitted to position out-of-plane into "up" ("U") or "down" ("D") configurations. Red dashed lines indicate the most primitive unit cells for each structure. (a) GrE-1, UUDDUD, (b) GrE-1, UUUDUD/DDDUDU, (c) GrE-2, UDUDUD, and (d) GrE-2, UUUDDD.

Establishing the Structure of GrE-2 Graphylene

We consider only structures that are naturally planar, i.e. have a top and bottom symmetry; for example, systems with inversion symmetry or mirror symmetry about the membrane plane have this property. If the top and bottom of the structure are different one expects the membrane to naturally curl. We avoid doing calculations on structures that are artificially stabilized by periodic boundary conditions by requiring top-bottom symmetry.

To evaluate structures we compute and compare the ground state (2D) enthalpy of our structures with respect to negative planar pressure. We compute this enthalpy by neglecting the out of plane dimension so that work is limited to be done in the membrane plane.

$$H_{2D} = U + p_{2D}A \tag{S1}$$

Where U is the internal energy, p_{2D} is the 2D analog of pressure (a force per unit length), and A is the area of the system. The internal energy, and 2D planar pressure and structure used to compute the enthalpies were all computed for the quantum mechanical ground state using first-principles DFT **[SR1, SR2]**.

We studied four GrE-2 structures. The first has PE chains with in-plane *cis*-conformations that give 6-fold rotational symmetry about the ring center as well as inversion symmetry; this corresponds to the hexagonal crystallographic layer group 75 (p 6/m) (Fig. S2a). The high rotational symmetry associated with this system suggests the PE chains have a handedness such that cycling around the C_6 ring the nearest bonds in the chains are orientated (RRRRRR), i.e. right-handed chirality. This configuration allows the methlyene bridges to optimally pack relative to each other, maximizing free volume for each atom. This system was stable and, based on its high symmetry and planar configuration, was considered a likely lowest-energy configuration.

The next hexagonal system we studied has PE chains with in-plane *cis*-conformations, but alternates chirality in an RLLRLL pattern (Fig. S2b). This oblique structure is associated with layer group 6 (p 1 1 2/m) and has 2-fold rotational symmetry about the C_6 ring centers and inversion symmetry. The RLLRLL system forces the atoms of neighboring methlyene groups into alternating regions of close and sparse proximity. This system was not stable and tended to force the PE cis-conformations to rotate out-of-plane in a stochastic manner, breaking symmetry. This structure is therefore clearly not preferred relative to the RRRRRR unit cell. However, the tendency for the PE bonds to rotate out-of-plane were suggestive that allowing such rotations could lead to stable structures. Note that other possible unit cells such as RLRLRL or RRRLLL cannot be symmetrically propagated within the hexagonal lattice geometry.

Therefore, we next considered a hexagonal system with 3-fold rotational symmetry about the ring center and inversion symmetry, but with PE chains with out-of-plane *cis*-conformations. This structure also has symmetry corresponding to layer group 66 (p -3) as shown in Fig. S2c. The symmetry of this system suggests the PE chains have an up- or down-orientation such that cycling around the C_6 ring gives orientations (UDUDUD). Like the RRRRRR structure, this structure is high symmetry and was found to have a stable, low-energy state. However the UDUDUD structure has a somewhat lower energy and higher density, suggesting that it would be a preferred configuration. Allowing the cis-conformations to orient out-of-plane reduces inter-atomic interference between neighboring PE chains, resulting in a lower energy state relative to RRRRRR.

We further studied lower symmetry structures based on out-of-plane *cis*-conformations, downselecting to the UUUDDD system (Fig. S2d). This system has out-of-plane PE *cis*-conformations and is somewhat analogous to hexagonal (p -3), however, the symmetry is rectangular. This structure has 2-fold rotational symmetry about one of its 2nd nearest neighbor axes (the same for all C_6 rings) and inversion symmetry and belongs to layer group 14 (p 2/m 1 1). This structure, compared to RRRRRR and UDUDUD structures, was found to have the highest areal density and lowest enthalpy, even to very high negative planar pressures. We were initially surprised to find that this less-symmetric UUUDDD structure was preferred relative to the highly symmetric UDUDUD structure, in particular considering that it forces methylene

groups in neighboring PE chains into closer proximity. However, the UUUDDD structure allows the C_6 rings to be tilted with respect to the membrane plane, enabling a more natural packing and higher density.

This UUUDDD GrE-2 structure was therefore selected for detailed fracture study. During MD simulations, we did not observe any systematic unit cell shifts into alternate configurations as the system was subject to thermal and strain excursions. Therefore, it is likely that UUUDDD is the preferred, lowest energy configuration for monolayer GrE-2. We note that our simulations are based on isolated polymer monolayers, rather than stacked or interacting sheets. It is possible that a simulation of stacked polymer crystallites would prefer the in-plane RRRRRR GrE-2 structure, rather than the UUUDDD or UDUDUD structures, due to its higher planarization and likely denser three-dimensional crystal structure. The study of 2D polymer ensembles and crystallites is a topic for further study.

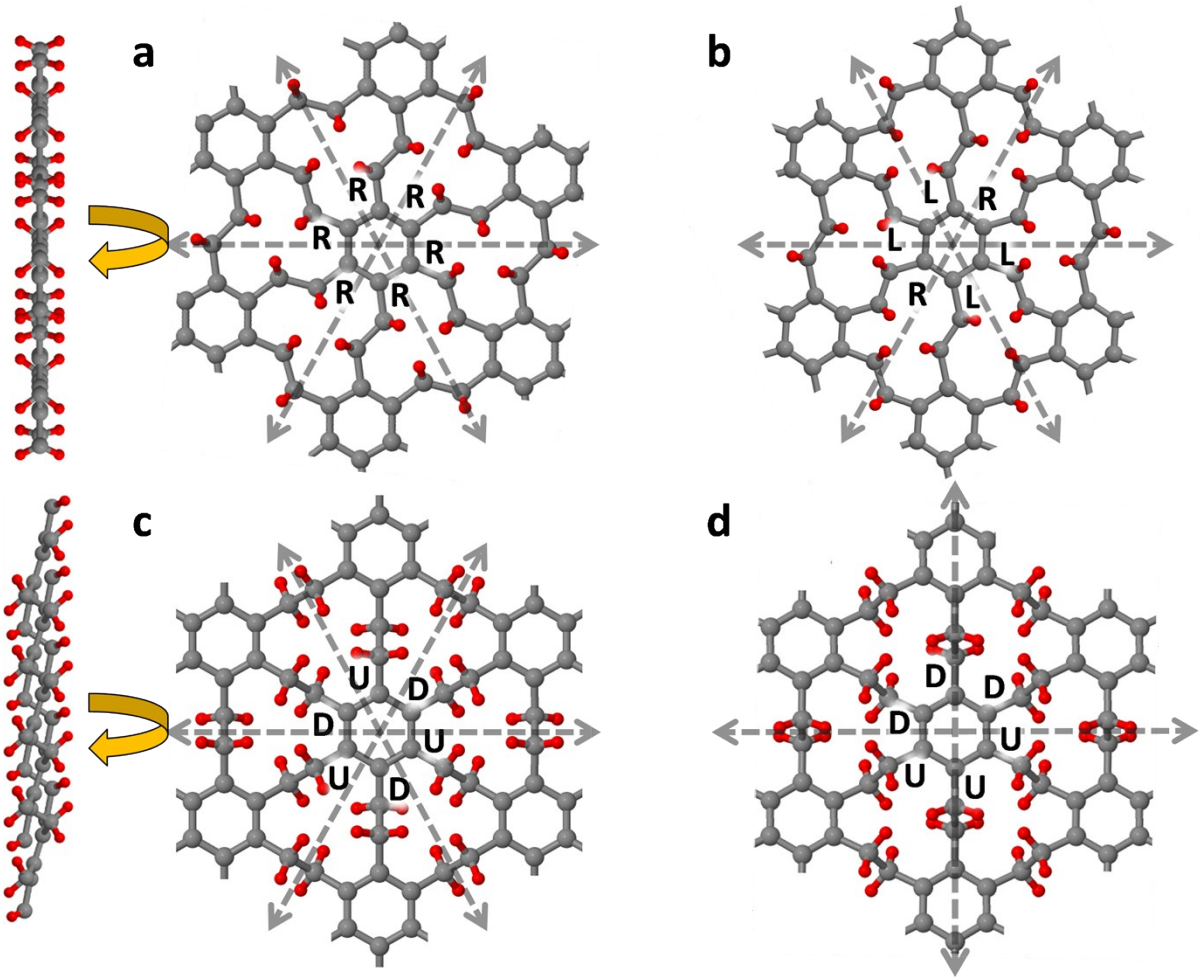

Figure S2. Comparison of GrE-2 unit cells considered. (a) RRRRRR, (b) RLLRLL, (c) UDUDUD, and (d) UUUDDD.

Relative 1NN and 2NN Stiffnesses for GrE-2

The GrE-2 structure demonstrates some anisotropy with respect to its mechanical properties, both at low strains and high strains. This behavior is in contrast to graphene, which is perfectly isotropic at infinitesimal strains, effectively isotropic at low strains (up to e.g. 5% strain), and only slightly anisotropic at high strains (e.g. 20-30%). The anisotropy in GrE-2 is due to the presence of the PE bridge groups. Figure S3 shows the resultant virial stresses in the GrE-2 system for loading in the 1NN and 2NN directions. It is evident that 1NN-direction loading is preferentially loading only the PE chains aligned in the 1NN direction, while 2NN-direction loading shares load between pairs of PE chains angled nominally at 30° relative to the 2NN direction.

We can crudely approximate this system as perfectly rigid C_6 rings joined by PE chains with spring constant *k*, with the nearest-neighbor distance between C_6 ring centers as *L* (at zero-strain state). Then for loading in the 1NN direction, we can define a unit cell of width $(\sqrt{3}/2) \times L$, over which one band of aligned PE chains is bearing most of the mechanical loads. We therefore have an effective modulus of

$$E_{1NN} = \frac{k}{(\sqrt{3}/2) \times L} \quad . \tag{S2}$$

In the 2NN direction, we define a unit cell of width *L* over which stiffness is provided by two PE chains, each oriented at 30° relative to the 2NN direction. The effective modulus in this direction is therefore

$$E_{2NN} = \frac{2(\sqrt{3}/2)k}{L} = \frac{\sqrt{3}k}{L} \quad . \tag{S3}$$

Combining eqns 2 and 3 gives an approximate stiffness ratio of E_{2NN}/E_{1NN} = 1.5.

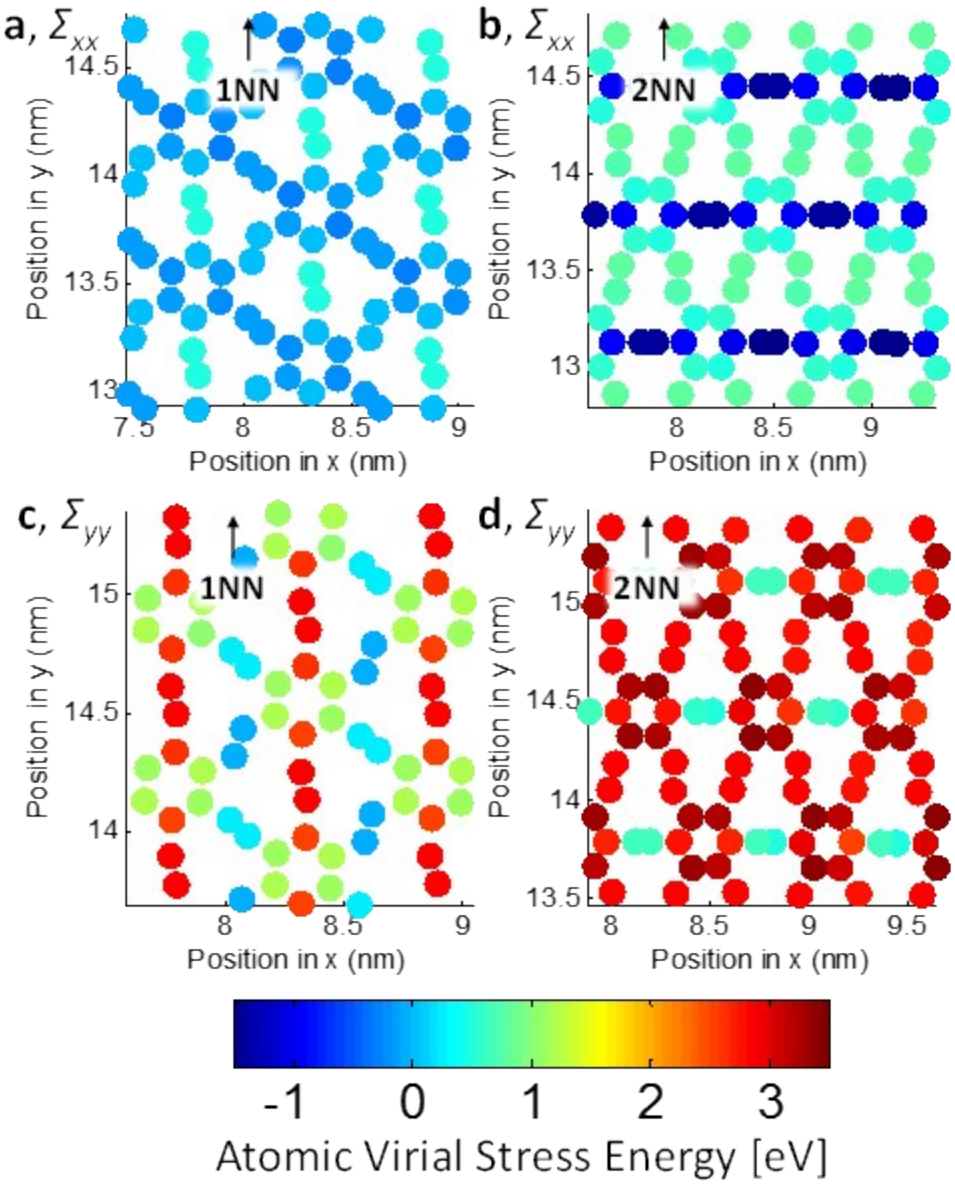

Figure S3. Comparison of tensile virial stresses at a strain of 12.5% for uniaxial stress loading in the (a) 1NN direction with x-axis stress reported, (b) 2NN direction with x-axis stress reported, (c) 1NN direction with y-axis stress reported and (d) 2NN direction with y-axis stress reported, as computed via MD.

Crack Tip Topology in GrE-2

When the crack tip radius in a fracture scenario is comparable to the size of the lattice constant of the material, the propagating crack tip is expected to converge to an intrinsic crack tip size and topology that are determined by the lattice size and architecture. This intrinsic crack tip size can provide useful insights into preferred fracture configuration and progression of the material.

To examine intrinsic crack tip topology, a minimal thickness ("sharp") crack was put into 60nm x 30nm domains of graphene and GrE-2, and the domains were stretched quasi-statically at 0K and a strain rate of $0.167ns^{-1}$. The crack was created by effectively “deleting” bonds across a 10nm line in the center of the domain. Since the AIREBO potential in LAMMPS is a pairwise potential, bonds are not explicitly defined in a master list. Rather, each atom determines its own bond-order and establishes thermodynamically-appropriate forces with its neighboring atoms. For our particular crack simulations, a bond can effectively be deleted in a pairwise potential by modifying the neighbor lists such that atoms on one side of a crack boundary do not “see” atoms on the other side of the crack boundary, and thus do not form bonds with them. In this way, we can create a sharp crack with minimal crack tip radius.

Creating a sharp crack allows us to examine crack tip topology for direct comparison between graphene and GrE-2. Figure S4a shows the relative performance of graphene and GrE-2 with sharp cracks and cracks with a finite radius if 1.5nm ("rounded" cracks). The sharp crack topology can be seen in Figure S4 with b) showing graphene at zero strain, c) showing graphene just before crack propagation, d) showing GrE-2 at no-strain and e) showing GrE-2 just before crack propagation.

The stress strain response shows that the fracture stress for graphene with a sharp crack is ~10% lower than the fracture stress for graphene with a rounded crack, while the sharp crack and rounded crack fracture strengths are comparable for GrE-2. The reduced fracture strength in graphene is associated with the higher stress concentration factor for the sharp crack versus the rounded crack, since the lattice constant for graphene is smaller than the 1.5 nm rounded crack tip radius. In contrast, the rounded crack tip is very similar in size to the lattice size of the GrE-2, so the sharp and rounded cracks demonstrate similar behaviors. This result shows that our crack initiation simulations using rounded cracks provide a conservative comparison of GrE-2 relative to graphene. Because of the smaller lattice constant in graphene, a propagating crack in graphene will converge to an intrinsic tip radius that is smaller than the intrinsic tip radius in GrE-2, increasing stress concentration effects and reducing the barrier to further crack propagation. This result suggests that increasing lattice constant in GrE-2 and similar 2D polymers is an effective technique for increasing fracture toughness.

Examining the topology of the crack tip in GrE-2 (Figure S4f), we see that a crack propagating along the 2NN direction encounters two ethylene chains that can share the crack tip stresses and rotate to accommodate local strain. In contrast, a crack propagating in the 1NN direction will focus the stress on a single ethlyene bond located at the crack tip (manuscript Figure 4b), leading to less deformation and energy absorption during crack propagation. A similar study of crack tip morphology and directional fracture dependence in graphene showed reduced stress intensity factors for cracks propagating along the zigzag direction compared to the armchair direction **[SR 18]**. This difference was due to the critical loading of a single, oriented sp^2 bond for zigzag cracks, compared to shared loading and rotation of two sp^2 bonds during incremental propagation of an armchair crack. A key distinction, however, is that in graphene there exists a crack path (zigzag direction) in which crack propagation can occur by failing a series of bonds perfectly normal to the crack path propagation direction, without any bond rotation required. In contrast, because of the topology of GrE-2 and the preference for failure through the sp^3 bonds, there exists no direction of fracture propagation in which failure occurs without bond rotation. Even along the preferred 1NN fracture direction, the ethylene groups are initially oriented at nominally

30° relative to the loading direction. Therefore bond rotation will also be an active mechanism during fracture in GrE-2, providing another mode of toughening that is not present in graphene.

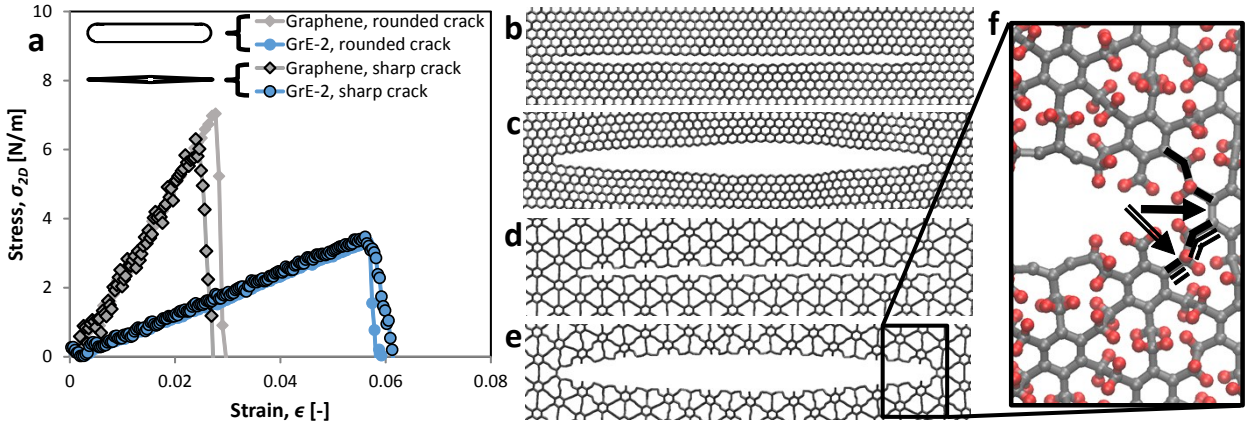

Figure S4: a) Stress-strain responses of graphene and GrE-2 with a rounded crack (r=0.15nm) and a sharp crack, b) sharp crack in graphene, c) sharp crack in graphene near rupture, d) sharp crack in GrE-2 (no hydrogen depicted for ease of viewing), e) sharp crack in GrE-2 near rupture, f) zoom-in of the crack tip in GrE-2 near rupture with a solid black arrow indicating an un-preferred crack growth direction, and the double-line black arrow indicating the preferred crack growth direction.

The method of creating a sharp crack in conjunction with Griffith crack theory can also be used to determine surface energy of a material. By simulating domains with cracks of varying length created using the aforementioned method and monitoring the system potential of each domain under a zero-strain condition with a separate crack size, it is possible to determine the surface energy, γ of the material using the simple relationship $\gamma = -d\prod/da$, assuming basic Griffith crack theory applies.

Mechanical Properties Relative to Conventional Engineering Materials

Table S1 shows tensile stiffness, strength, density, and density-normalized strength for graphene, GrE-2, Kevlar yarns, and titanium. GrE-2 data is presented in 1NN and 2NN directions, as well averaged property values representing a directional average. Graphene and GrE-2 strength, stiffness, and density are listed as two-dimensional values, but when normalized provide specific strength and stiffness values that are of equivalent units to the values calculated for Kevlar and titanium based on three-dimensional properties. The data shows that GrE-2 has a specific stiffness that is 2× higher than Kevlar and 5× higher than titanium; and a specific strength that is 9× higher than Kevlar and 50× higher than titanium.

Table S1. Comparison of mechanical properties for graphene, GrE-2, Kevlar yarns, and titanium. All property values for graphene Kevlar, and titanium is from [SR 17].

Material	Stiffness (N/m)	Strength (N/m)	Density (kg/m^2)	Specific stiffness (GPa/(kg/m^3))	Specific strength (GPa/(kg/m^3))
Graphene	329	35.8	7.42E-07	443	48.2
GrE-2 1NN	78.9	11.4	6.53E-07	121	17.5

GrE-2 2NN	97.6	16.4	6.53E-07	150	25.1
GrE-2 average	88.3	13.9	6.53E-07	135	21.3

Material	**Stiffness** (GPa)	**Strength** (GPa)	**Density** (kg/m^3)	**Specific stiffness** ($GPa/(kg/m^3)$)	**Specific strength** ($GPa/(kg/m^3)$)
Kevlar	96	3.38	1440	66.7	2.35
Titanium	114	1.86	4430	25.7	0.420

References

SR1 P. Hohenberg, W. Kohn. “Inhomogeneous Electron Gas” Phys. Rev. v136, B864. 1964.

SR2 W. Kohn, L. J. Sham. “Self-Consistent Equations Including Exchange and Correlation Effects” Phys. Rev. v140, A1133. 1965.

SR3 CP2K Open Source Molecular Dynamics, http://www.cp2k.org/.

SR4 J. VandeVondele, M. Krack, F. Mohamed, M. Parrinello, T. Chassaing, and J. Hutter. “QUICKSTEP: Fast and accurate density functional calculations using a mixed Gaussian and plane waves approach." Comp. Phys. Commn. v167 p103. 2005.

SR5 A. D. Becke. “Density-functional exchange-energy approximation with correct asymptotic behavior.” Phys. Rev. A. v38 p3098-3100. 1988.

SR6 C. Lee, W. Yang, and R. G. Parr. “Development of the Colle-Salvetti correlation-energy formula into a functional of the electron density.” Phys. Rev. B. v37 p785-789. 1988.

SR7 S. Goedecker, M. Teter, and J. Hutter. “Separable dual-space Gaussian pseudopotentials.” Phys. Rev. B. v54 p1703-1710. 1996.

SR8 C. Hartwigsen, S. Goedecker, and J. Hutter. “Relativistic separable dual-space Gaussian pseudopotentials from H to Rn.” Phys. Rev. B. v58 p3641-3662. 1998.

SR9 M. Krack. “Pseudopotentials for H to Kr optimized for gradient-corrected exchange-correlation functionals.” Theor. Chem. Acc. v114 p145-152. 2005.

SR10 S. Grimme. “Semiempirical GGA-type density functional constructed with a long-range dispersion correction." J. Comp. Chem. v27 n15 p1787-1799. 2006.

SR11 S. Grimme, J. Antony, S. Ehrlich and H. Krieg. “A consistent and accurate ab initio parametrization of density functional dispersion correction (DFT-D) for the 94 elements H-Pu.” J. Chem. Phys. v132 p154104. 2010.

SR 12 LAMMPS Open Source Molecular Dynamics http://lammps.sandia.gov

SR 13 S.J. Stuart, A.B. Tutein, and J.A. Harrison, “A reactive potential for hydrocarbons with intermolecular interactions.” J. of Chem. Phys. V112. p6472-6486. 2000.

SR 14 R. Grantab, V.B. Shenoy, and R.S. Ruoff, “Anomalous Strength Characteristics of Tilt Grain Boundaries in Graphene.” Science. v330 p946-948. 2010.

SR 15 P. Zhang, et al., “Fracture toughness of graphene.” Nat. Comm. v5. 2014.

SR 16 Q. Pei, Y. Zhang, and V. Shenoy, “A molecular dynamics study of the mechanical properties of hydrogen functionalized graphene.” Carbon. v48 p898-904. 2010.

SR 17 E.D. Wetzel, R. Balu, and T.D. Beaudet, “A theoretical consideration of the ballistic response of continuous graphene membranes.” J. Mech. Phys. of Sol. v82 p23-31. 2015.

SR 18 D. Datta, S.PV. Nadimpalli, Y. Li, V.B. Shenoy, “Effect of crack length and orientation on the mixed-mode fracture behavior of graphene”, Ex. Mech. Let. V5 p10-17. 2015.